Model-based design of a mechanically intelligent shape-morphing structure

Chen, Qianyi; Schott, D.L.; Jovanova, J.

DOI
10.1038/s41598-024-74379-4

Publication date
2024

Document Version
Final published version

Published in
Scientific Reports

scientific reports

Check for updates

OPEN

Model-based design of a mechanically intelligent shape-morphing structure

Qianyi Chen✉, Dingena Schott & Jovana Jovanova

Soft robotics has significant interest within the industrial applications due to its advantages in flexibility and adaptability. Nevertheless, its potential is challenged by low stiffness and limited deformability, particularly in large-scale application scenarios such as underwater and offshore engineering. The integration of smart materials and morphing structures presents a promising avenue for enhancing the capabilities of soft robotic systems, especially in large deformation and variations in stiffness. In this study, we propose a multiple smart materials based mechanically intelligent structure devised through a model-based design framework. Specifically, the intelligent structure incorporates smart hydrogel and shape memory polymer (SMP). Employing the finite element method (FEM), we simulated the complex interactions among smart material to analyze the performance characteristics of the intelligent structure. The results demonstrate that, utilizing smart hydrogel and shape memory polymer (SMP) can effectively attain large deformation and exhibit variable stiffness due to the shape memory effect. Besides, the shape-morphing structures exhibit customized behaviours including bending, curling, and elongation, all while reducing reliance on external power sources. In conclusion, utilizing multiple smart materials within the model-based design framework offers an efficient approach for developing mechanically intelligent structure capable of complex deformations and variable stiffness, thereby providing support for underwater or offshore engineering applications.

Keywords Mechanically intelligent structure, Model-based design, Shape morphing, Hydrogel, Shape memory polymer, Finite element method (FEM)

List of symbols

C_1, C_2	Material constant
C_{A^-} $(\mathrm{mol/m})^3$	Fixed charge group concentration
C_{AH} (mol/m^3)	Associated acidic group concentration
C_{H^+}, C_+, C_- $(\mathrm{mol/m})^3$	Nominal concentrations of hydrogen ions, mobile cations, anions
c_{H^+}, c_+, c_- $(\mathrm{mol/m})^3$	True concentrations of cations, anions and hydrogen ions inside
$\overline{c}_{H^+}$, $\overline{c}_+$, $\overline{c}_-$ $(\mathrm{mol/m}^3)$	True concentrations of cations, anions and hydrogen ions outside
C_s (mol/m^3)	Concentration of solvent
d_i (mm)	Diameter of different hydrogel element
E_n (MPa)	Instantaneous modulus
E_i (MPa)	Elastic modulus
e'	Dimensionless number represent length change
F_{ik}	Deformation gradient of the network
F_E (N)	External force
f	Number of acidic groups on a polymer chain
K_a	Constant of acidic dissociation
h (mm)	Height of each block unit
k (J·K^{-1})	Boltzmann constant
L_h, L_v	Total layers in horizontal direction, total layers in vertical direction
L_s (mm)	Distance from the top end to the bending point
N	The polymer chains number divided by the volume of the dry network

Faculty of Mechanical Engineering, Delft University of Technology, Delft 2628 CD, The Netherlands. ✉email: Q.Chen-5@tudelft.nl

N_A (mol^{-1})	Avogadro number
v_s (m^3)	Single molecule volume
S_a (N·mm/rad)	Bending stiffness
T (K)	Absolute temperature
T_g (K)	Glass transition temperature
T_r (K)	Reference temperature
t (S)	Time
P_h, P_v (mm)	The lengths of the structure in horizontal and vertical direction
w (J/m^3)	Free energy density
μs (J/mol)	Chemical potential
Π_{sol}, Π_{ion} (Pa)	Osmotic pressures from polymer-solvent, ion-solvent mixtures
ε_0	Strain at the initial time
ξ_t (mm)	Diameter difference
ξ_d (mm)	Thickness difference between two surface
θ (deg)	Rotational angle caused by the external moment
φ (deg)	bending angle

Soft robotics demonstrates significant superiority in advanced flexibility and adaptability, making it applicable across various industrial domains[1–3]. Soft actuators, serving as primary energy sources for soft robotic systems, can be classified into several conventional forms, including electrical, pneumatic, particle jamming, and chemically-driven actuators[4–7]. However, conventional actuation techniques frequently require supplementary power sources, thereby constraining their versatility. Smart materials, characterized by unique functionalities, present innovative opportunities for enhancing the development of flexible and adaptable soft actuators[8]. Smart materials can change their structure or composition in response to various external stimuli, including electricity, magnetic fields, light, heat, or chemical reactions[9–11].

Among the smart materials utilized in soft robotics, smart hydrogels are widely used owing to the improved mechanical flexibility and suitability for a range of material substrates[12]. Owing to their polymer structure, being cross-linked either physically or chemically, hydrogels show as elastic solids characterized by deformability and softness[13]. Smart hydrogel have the ability to swell or shrink in response to external stimuli, primarily including factors such as temperature, pH, light, or chemical triggers[14]. Within the special attributes, smart hydrogels can be easily integrated into soft robotics systems to serve as actuators. Zheng et al.[15] demonstrated a soft gripper comprising a bilayer structure, capable of functioning even in the air conditions, achieved by layering two distinct types of temperature-responsive hydrogels. Duan et al.[16] developed a soft actuator that produces significant deformations and demonstrates bidirectional bending by stacking anionic and cationic pH-responsive hydrogels. Takashima et al.[17] developed an expansion–contraction artificial muscle utilizing photo-responsive hydrogel. Palleau et al.[18] created a reversible hydrogel actuator that can grasp small objects in ethanol (EtOH) and release them in water. However, despite their flexibility, the low modulus and mechanical strength of the hydrogels limit their application in complex environments and stiffness variation. Furthermore, shape memory polymers (SMPs) are another smart materials widely employed as actuators, which are crucial components in soft robotics devices for enhancing stiffness[19,20]. Their functionality is based on the principle of phase transition, which changes the relative mechanical properties and achieve self-healing or shape memory effect[21]. SMPs respond to various stimuli, with temperature being the most common. Specifically, when exposed to temperatures above their transition point, SMPs change from a glassy phase to a rubbery phase. In the rubbery phase, SMPs exhibit a low elastic modulus, supporting them highly deformable. When SMPs cool and return to the glassy phase, they retain the deformed shape, recovering a high elastic modulus and thus achieving stiffness variation[22]. Gandhi et al.[23] introduced a multilayer configuration utilizing SMP, featuring adaptable stiffness by changing the state of the polymer. Wang et al.[24] proposed a bioinspired soft robotic finger based on the SMP, featuring adaptable bending capabilities by controlled adjustments in stiffness. Despite exhibiting unique function and shape control, most SMPs only have one-way shape memory effect and lack the ability to deform in response to stimuli triggers. Thus, SMP-based designs need external loading to achieve desired deformations.

In complex environments or spaces, soft robots are required to carry out tasks including grasping, exploration, and transportation[25–27]. However, developing tailored morphing structures with complicated deformation capabilities is often limited by the complexity and inefficiency of experimental research. Alternatively, numerical simulations offer a more efficient approach to predict and describe the deformation behaviours[28,29]. Soft actuators present considerable challenges in modeling because of their significant nonlinear characteristics and complex geometries. The finite element method (FEM), extensively employed in modeling nonlinear mechanics, offers an effective approach for overcoming these challenges without requiring explicit analytical frameworks[30]. Nyuyen et al.[31] developed a model for a soft actuator applied in the wearable assistive devices. Song et al.[32] proposed a SMP-based adaptable gripper inspired by octopus morphology, employing numerical modeling techniques to develop versatile configurations. Given the challenges and expenses associated with fabricating complex shape structures, employing FEM as a computational approach to simulate various smart materials proves to be an efficient strategy[33]. However, the deformability of soft actuator structures depends on hyperelastic nonlinear materials. Therefore, the material model used in simulations must be calibrated to relevant strain levels for the applications.

This study presents the design of a mechanically intelligent shape-morphing structure incorporating smart materials to achieve tailored deformation and stiffness variation. The contributions of this work include several points. First, the novel intelligent structure unit, based on the combination of pH-sensitive hydrogel and SMP, is designed to achieve volume and stiffness variation. Then, the building block of different shape-morphing structures based on the smart units are proposed for applications in soft robotics. Furthermore, To

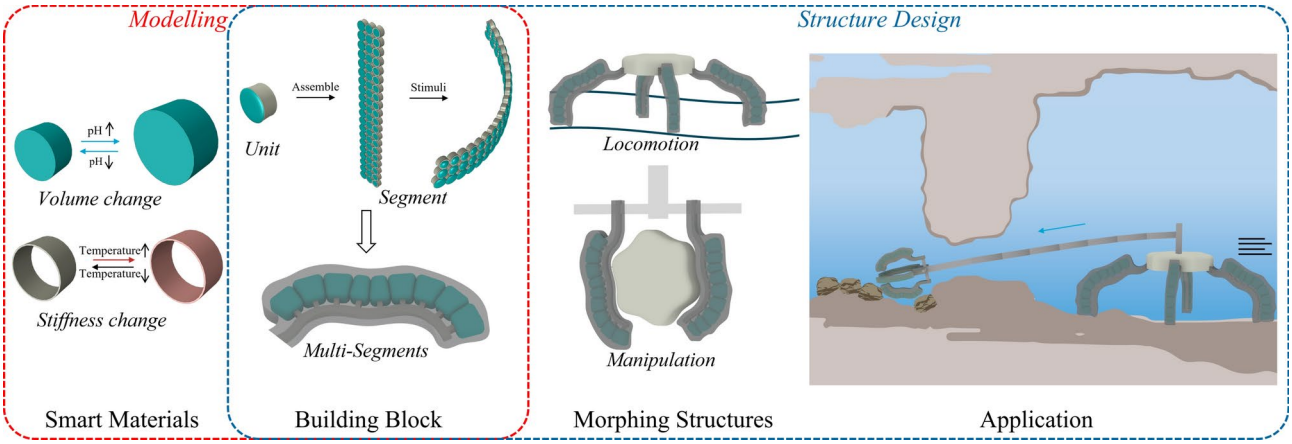

Fig.1. The design framework by building blocks.

effectively capture large deformations while also reducing computational costs, we used a novel approach. Here the constitutive model, combined with a simplified viscoelastic model, is used in the FEM solver to describe the nonlinear behaviours of both pH-sensitive hydrogel and SMP within the same structure. The design strategy is illustrated in Fig. 1. Initially, the intelligent structural unit is created using multiple smart materials. Subsequently, the numerical approach is applied to investigate the different deformation behaviors of building blocks, which are composed of intelligent units. Based on these building blocks, morphing structures are then developed through structural design to achieve specific functionalities. Moreover, these morphing structures have potential applications in soft robotics, such as in grasping tasks during undersea cave exploration, where they could be used for ore collection.

Methodology

The modeling of smart materials holds significance in design processes. This study employs Finite Element Method (FEM) to describe the nonlinear characteristics of the pH-sensitive hydrogel and thermal response Shape Memory Polymer (SMP). pH-sensitive hydrogel and SMP are utilized as the smart materials integrated into the actuator. The pH-sensitive hydrogel is selected as the smart actuating material that can be used underwater due to their low cost, and high adaptability and sensitivity. In addition, the elevated pH levels in seawater, as opposed to air, create optimal conditions for activating pH-sensitive hydrogels. This property makes pH-sensitive hydrogels ideal materials for use in ocean engineering applications.Similarly, SMP is chosen based on the simplicity of achieving triggering conditions. The swelling and shrinking of the hydrogel induced to actuate the structure, while the shape memory effect of SMP applied as the stiffness enhanced method.

The pH-sensitive hydrogel modelling

Hydrogel exhibits hyperelastic properties and can be described by free energy theory to understand diffusion and deformation mechanisms[34]. The free energy density of pH-sensitive hydrogels encompasses various contributing factors and expressed as,

$$W\left(\mathbf{F}, C_{H^+}, C_+, C_-\right) = W_{net}\left(\mathbf{F}\right) + W_{sol}\left(\mathbf{F}\right) + W_{ion}\left(\mathbf{F}, C_{H^+}, C_+, C_-\right) + W_{dis}\left(\mathbf{F}, C_{H^+}, C_+, C_-\right), \tag{1}$$

where W is the free energy density, $\mathbf{F}$ denotes the deformation gradient tensor, and C_{H^+}, C_+, C_- are nominal concentrations of hydrogen ions, mobile cations, anions, respectively. $W_{net}\left(\mathbf{F}\right)$ is the elastic energy from polymer network stretching, that can be expressed by Neo-Hookean model as,

$$W_{net}\left(\mathbf{F}\right) = \frac{NkT}{2}\left[F_{ik}F_{ik} - 3 - 2\log(\det\mathbf{F})\right], \tag{2}$$

where N is the polymer chains number divided by the volume of the dry network, F_{ik} is the deformation gradient of the network, and the swelling volume is, $\det\mathbf{F} = 1 + v_s C_s$, where C_s and v_s are the concentration of solvent and single molecule volume, respectively. Moreover, k is the Boltzmann constant and T is the absolute temperature. $W_{sol}\left(\mathbf{F}\right)$ is from polymer–solvent mixing and described by Flory–Huggins model[35,36],

$$W_{sol}\left(\mathbf{F}\right) = \frac{kT}{v_s}\left[\left(\det\mathbf{F} - 1\right)\log\left(1 - \frac{1}{\det\mathbf{F}}\right) - \frac{\chi}{\det\mathbf{F}}\right], \tag{3}$$

where χ is the Flory–Huggins interaction coefficient, expressing the enthalpy of the mixing polymer. $W_{ion}\left(\mathbf{F}, C_{H^+}, C_+, C_-\right)$ represents energy from ion–solvent, and mobile ions, with their low concentration, primarily affect free energy through mixing entropy,

$$W_{ion}\left(\mathbf{F}, C_{H^+}, C_+, C_-\right) \\ kT\left[C_{H^+}\left(\log\frac{C_{H^+}}{C_{H^+}^{ref}\det\mathbf{F}}-1\right)+C_+\left(\log\frac{C_+}{C_+^{ref}\det\mathbf{F}}-1\right)+C_-\left(\log\frac{C_-}{C_-^{ref}\det\mathbf{F}}-1\right)\right], \tag{4}$$

and $W_{dis}\left(\mathbf{F}, C_{H^+}, C_+, C_-\right)$ arises from acidic group dissociation in polymer chains,

$$W_{dis}\left(\mathbf{F}, C_{H^+}, C_+, C_-\right) = kT\left[C_{A^-}\log\left(\frac{C_{A^-}}{C_{A^-}+C_{AH}}\right)+C_{AH}\log\left(\frac{C_{AH}}{C_{A^-}+C_{AH}}\right)\right]+\gamma C_{A^-}, \tag{5}$$

where γ denotes the enthalpy increase, while C_{A^-} and C_{AH} represent fixed charge and associated acidic group concentration. The relationship between these concentrations requires, $C_{A^-}=C_{H^+}+C_+-C_-$, and $C_{AH}=f/v_s-\left(C_{H^+}+C_+-C_-\right)$, in which f is the number of acidic groups on a polymer chain. The thermodynamic state of the system is entirely determined by the free energy, as described by Eq. (1). Once the explicit expression of the system's free energy is obtained, the elastic stress of the hydrogel can be derived as,

$$\sigma_{ij}=\frac{F_{jK}}{\det\mathbf{F}}\frac{\partial\left(W_{net}+W_{sol}+W_{dis}\right)}{\partial F_{iK}}-\frac{\mu_s}{v_s}\delta_{ij}, \tag{6}$$

where μ_s represents the chemical potential. Using the osmotic pressure to express μ_s, the stress tensor can be expressed as,

$$\sigma_{ij}=\frac{NkT}{\det\mathbf{F}}\left(F_{ik}F_{jk}-\delta_{ij}\right)-\left(\Pi_{sol}+\Pi_{ion}\right)\delta_{ij} \tag{7}$$

The osmotic pressures from polymer–solvent and ion–solvent mixtures, denoted Π_{sol}, and Π_{ion}, respectively, are defined as,

$$\Pi_{sol}=-\frac{kT}{v_s}\left[\log\left(1-\frac{1}{\det\mathbf{F}}\right)+\frac{1}{\det\mathbf{F}}+\frac{\chi}{(\det\mathbf{F})^2}\right], \tag{8}$$

$$\Pi_{ion}=kT\left(c_{H^+}+c_++c_--\overline{c}_{H^+}-\overline{c}_+-\overline{c}_-\right), \tag{9}$$

where $c_i\,(i=+,-,H^+)$ and $\overline{c}_i\,(i=+,-,H^+)$ describe the true concentrations of cations, anions and hydrogen ions inside and outside, respectively. In addition, the true concentrations and nominal concentrations are related as, $C_i=c_i\det\mathbf{F}$. The $\overline{c}_{H^+}$ also relates to the pH of outside solution and is expressed as,

$$\overline{c}_{H^+}=N_A10^{-\overline{\mathrm{pH}}} \tag{10}$$

where N_A is the Avogadro number, $N_A=6.023\times10^{23}$. In addition, the specific conditions are required for ionic equilibrium as[37],

$$\frac{c_+}{\overline{c}_+}=\frac{\overline{c}_-}{c_-}=\frac{c_{H^+}}{\overline{c}_{H^+}} \tag{11}$$

By applying the Donnan equations and considering the principle of electroneutrality within the hydrogel, the following equation for acid dissociation is derived,

$$\frac{c_{H^+}\left(c_{H^+}+c_++c_-\right)}{\left(\frac{f}{v_s}\right)(\det\mathbf{F})^{-1}-\left(c_{H^+}+c_++c_-\right)}=N_AK_a \tag{12}$$

where K_a is constant of acidic dissociation. Equation (12) is expressed based on c_{H^+} that can be solved FEM solver. In the numerical simulation process, the Abaqus finite element solver is employed for the pH-sensitive hydrogel. A user-defined subroutine is utilized to describe the hyperelastic material based on the free energy function. It is assumed in this model that the volume per monomer is equivalent to the volume per solvent molecule. Additionally, the composition of the external solution is defined solely by $\overline{c}_+$ and $\overline{c}_{H^+}$. The electroneutrality in the outside solution needs to satisfy $\overline{c}_-=\overline{c}_++\overline{c}_{H^+}$, where $\overline{c}_{H^+}$ is considered as a variable calculated from the input pH value.

SMP modelling

The shape memory effect relating to the stiffness variation shows significant viscoelsticity, spanning temperatures both above and below the glass transition temperature[38,39]. In our study, we employed the superimposed generalized Maxwell model and Williams-Landel-Ferry (WLF) equation within Abaqus finite element solver to elucidate the mechanical behavior of SMP. The utilized constitutive equations for the multi-branch viscos-elasticity are as follows[40],

$$\sigma\left(t\right)=\varepsilon_0E_n+\varepsilon_0\sum_{i=1}^{n-1}E_ie^{\frac{-t}{\tau_i}} \tag{13}$$

where $\sigma\left(t\right)$ represents stress at time *t*, ε_0 is the strain at the initial time,E_n denotes the instantaneous modulus, E_i and τ_i represent the elastic modulus and relaxation time of the Maxwell element *i*, respectively.

The relation of relaxation modulus E in the generalized Maxwell equation with time t is expressed as follows,

$$E(t) = E_n + \sum_{i=1}^{n-1} E_i e^{\frac{-t}{\tau_i}} \tag{14}$$

and satisfies the limit condition, $\lim_{t\to\infty} E(t) = E_n$. Conducting relaxation experiments at various temperatures and applying the time–temperature equivalence principle is essential. This allows the conversion of the relaxation response curve of SMP across different temperatures into a comprehensive relaxation response curve at a specific temperature. According to the WLF Eq. [40], the connection between the relaxation time at the present temperature T and the relaxation time at the reference temperature of T_r can be written as,

$$lg\alpha_T = lg\frac{\tau}{\tau_r} = \frac{-C_1(T-T_r)}{C_2+(T-T_r)} \tag{15}$$

where α_T represents shift factor, C_1 and C_2 are material constant. And it is assumed that here the glass transition temperature (T_g) is same as T_r.

Simulation setup

For the specific materials, poly(acrylic acid) (PAA) hydrogel, a widely recognized pH-sensitive hydrogel, is used as a reference in this study, with the polymer specified by several parameters. In particular, the representative value of volume of per water molecule is $v_s = 10^{-28}m^3$, and the number of monomers per chain is $1/Nv_s$. The chemical potential, normalized by kT, is 4×10^{-21} J. For the PAA hydrogel, which exhibits a preference for large swelling ratios, the parameters Nv_s , f, and χ are set to 0.001, 0.03, and 0.1, respectively. Additionally, the concentrations of anions $\bar{c}_-$ is 0.005 M and dissociation constant K_a is $10^{-4.3}$, both of which are typical for carboxylic acids[37]. The pH is set as the input parameter, which changes from 2 to 8. Furthermore, polylactic acid (PLA), recognized for its biodegradability, non-toxicity, and renewability, is selected as SMP for modeling[41]. The parameters related to the viscoelastic and thermal properties are set as, $T_g = 334\text{K} C_1 = 6.14$ and $C_2 = 293\text{K}$ [42]. The material's elastic modulus was 1000 MPa at 298 K, decreasing by 60% at the transition temperature[43]. Consequently, the temperature range from 295 to 360 K was selected for the simulation.

For the remaining configurations, a standard 3D C3D8H mesh (8-node linear brick, hybrid with constant pressure) was selected to enhance mesh quality and convergence by addressing thin and irregular edges. Grid independence verification confirms global mesh sizes at around 0.5. Emphasis was exclusively placed on morphing structures in designing, with gravitational impact disregarded.

Mechanical intelligent structure design and validation

The working principle of the proposed soft intelligent structure is illustrated in Fig. 2. It consists of a pH-sensitive hydrogel cylinder covered by the SMP ring. In the simulation, the tied constraint interface is used between the hydrogel and SMP cover. Initially, at low pH and high temperatures above the transition point, the hydrogel is shrunken and the SMP is in a rubbery state. When the pH rises, the hydrogel expands, leading to the deformation of the SMP cover as a result of the hydrogel's increased volume. Once the hydrogel has fully expanded, reducing the temperature below the transition point enhances the stiffness of the SMP cover, locking the deformed shape. By subsequently raising the temperature and lowering the pH, the hydrogel contracts back to its original volume, allowing the SMP frame to return to its initial size. Therefore, the SMP frame is classified as a one-way shape memory material, which undergoes deformation through the activation of the hydrogel. By using this soft intelligent structure as the unit cell, various shape-morphing structures can be developed. Besides, the self-actuation strategy independent of specialized equipment will be implemented in practical applications.

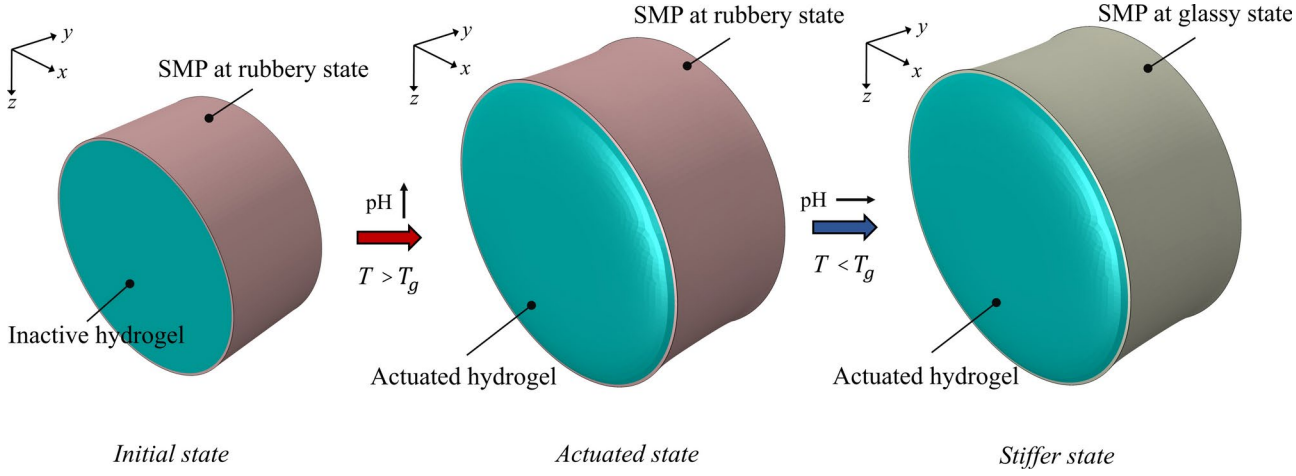

Fig. 2. The working principle of the intelligent structure.

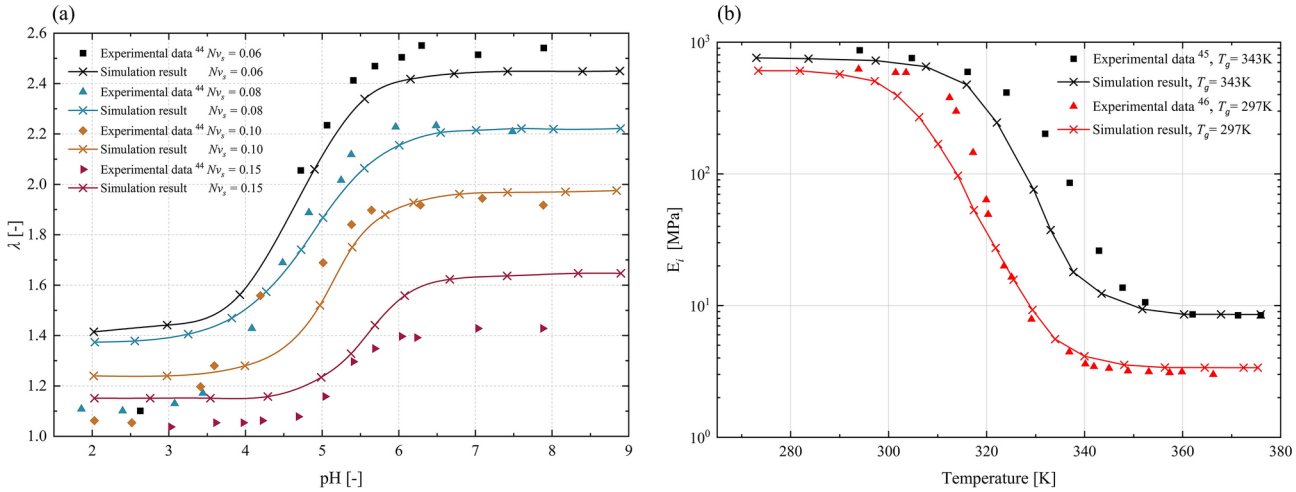

Fig. 3. The comparison of smart materials' properties between experimental data and simulation results. (**a**) The swelling ratio (λ) changes of hydrogel by pH. (**b**) The elastic modulus (E_i) changes of SMPs by temperature.

	Initial	Step 1	Step 2	Step 3	Step 4	Step 5	Step 6	Step 7
pH (-)	2	3	4	5	6	7	8	8
Temperature (K)	360	360	360	360	360	360	360	295

Table 1. The stimuli parameters during simulation steps.

The developed intelligent structure will be utilized in maritime and offshore engineering, where environmental conditions will actuate the hydrogels and SMP. For instance, high pH seawater can cause the hydrogel to swell, while hot gases released from ships or undersea construction can trigger the phase transition of SMPs. Consequently, this self-actuation process conserves resources and leads to mechanically intelligent systems.

Furthermore, To validate the materials model, the simulated behaviour of different pH sensitive hydrogels and typical SMPs are compared to experimental data. The comparison of pH sensitive hydrogels are shown in Fig. 3a. Different experimental data with different crosslink density was presented by Eichenbaum et al.[44]. In addition, Nv_s is set from 0.06 to 0.15 to match with the experimental setup. Correspondingly, the matchable materials parameters are given as, $\overline{c}_- = 0.03\mathrm{M}$, $K_a = 10^{-4.7}$, and $f = 0.35$. The simulation results have the similar trend with the experimental data. The swelling ratio (λ) of the hydrogel rises proportionally with pH, while the increase in Nv_s leads to the reduction in λ. The comparison between the simulation results and experimental data for SMPs is shown in Fig. 3b. The experimental data with T_g of 343 K was obtained by Liu et al.[45], while the experimental data with T_g of 297 K was obtained Qi et al.[46]. To align the simulation with the experimental data from Liu et al., the material parameters were set to, $C_1 = 14.8$ and $C_2 = 317.4\mathrm{K}$. Similarly, for comparison with Qi et al.'s experimental data, the simulation parameters were set to, $C_1 = 7$ and $C_2 = 297\mathrm{K}$. The simulation results exhibit acceptable agreement with experimental data, demonstrating a significant decrease in the elastic modulus of SMPs as temperature rises. Despite differences between simulations and experimental results, the qualitative behavior of the hydrogel and SMP can prove the working principle, making the simulations sufficient.

Results and discussion

In this section, we propose and analyze morphing structures composed of multiple intelligent units. Simulations are conducted for all cases across a pH range of 2 to 8. Initially, the temperature is set to 360 K to ensure that the SMP remains in a rubbery state. After the hydrogel has fully swollen under a pH of 8, the temperature is lowered to 295 K to lock the shape. The detailed parameters are provided in Table 1. Initially, the hydrogel is in a low-swelling state, while the temperature is maintained above the SMP transition temperature of 360 K to facilitate deformation. From steps 1 to 6, the temperature remains elevated, while the pH is gradually increased from 2 to 8, causing the hydrogel to swell. In the final step, the temperature is lowered below the SMP transition temperature to 295 K, allowing the SMP to enter a glassy state, thereby locking the morphed shape in place.

Case studies: bending, curling and elongation structures

Various building blocks can be developed by integrating basic intelligent units, such as bending, curling, and elongation configurations. Furthermore, to attain tailored deformation behaviors in different configurations, the primary design principle involves varying the thickness of the SMP frame, while maintaining the uniformity of other structural components. Specifically, the thickness of SMP frame includes the thickness of ring shaped unit and the thickness of different side within each unit.

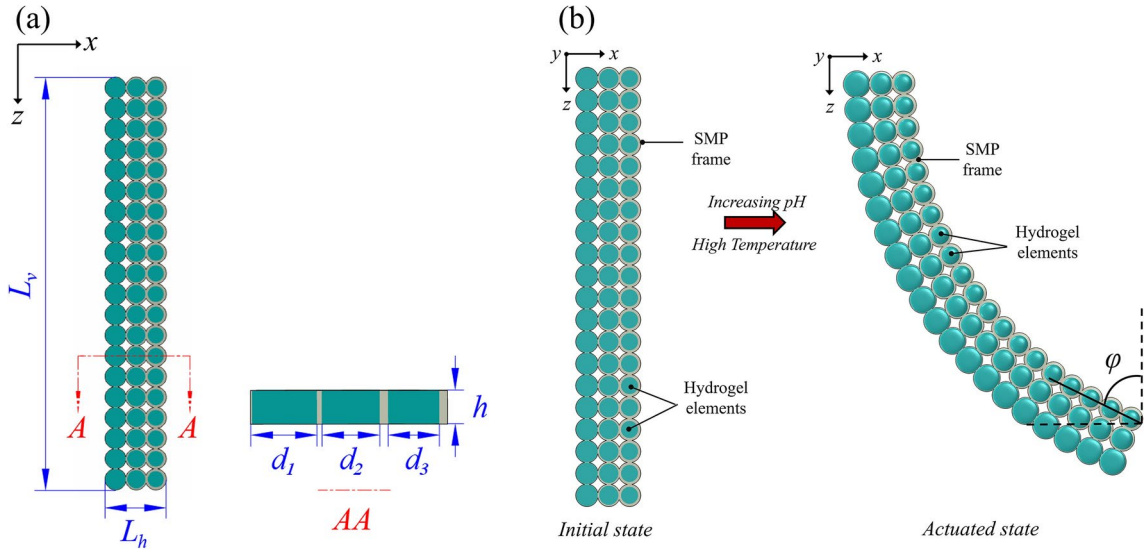

Fig. 4. The shape-morphing structure: bending building block (**a**) structural design (**b**) working principle.

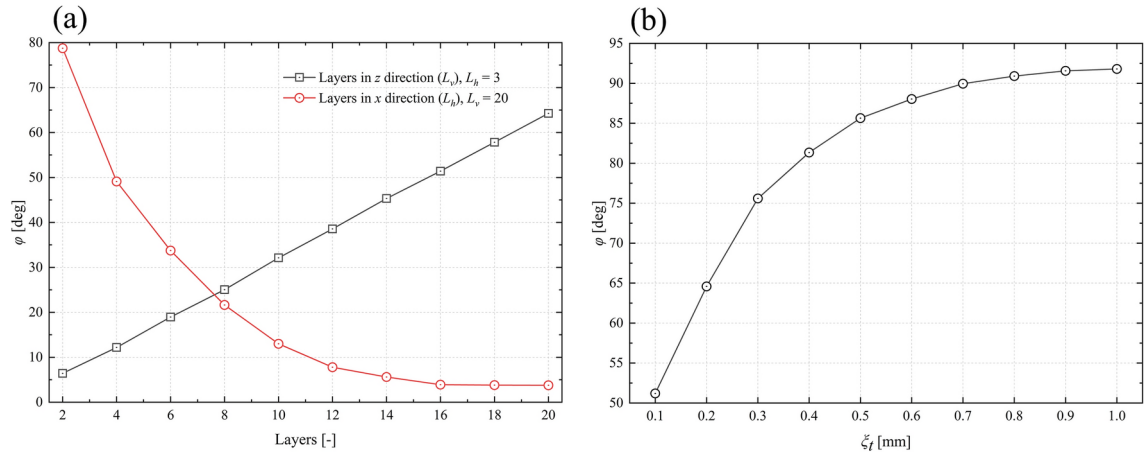

Fig. 5. The bending performance affected by different influential parameters. (**a**) The bending angle (φ) changes by building block layers. (**b**) The bending angle (φ) changes by thickness difference (ξ_t) under the condition: Lh = 3, Lv = 20.

The building block of bending configuration is shown in Fig. 4. The structural design is shown in Fig. 4a. Based on the intelligent unit, SMP rings of different thicknesses are used to overlap each other to form an overall structure. In the designed structure, the total layers in z direction (L_v) is used to show the length, and the total layers in x direction (L_h) is to describe the width. Besides, the diameter of each cylinder unit and height (h) of each block unit are 20 mm and 10 mm, respectively. The diameter difference ξ_t is illustrated as,

$$d_{i+1} - d_i = \xi_t \tag{16}$$

where d_i denotes the diameter of different hydrogel element.

The working principle of the bending structure is illustrated in Fig. 4b. Upon actuating the hydrogels with the rubbery state SMP, the block unit swells variably due to ξ_t. This differential swelling causes the morphing structure to bend in the x direction. The shape is then locked by lowering the temperature, transitioning the SMP to a glassy state. The bending performance is quantified by the bending angle (φ).

The bending performance affected by different influential parameters is explored, shown in Fig. 5. The bending performance affected by different structure layers is shown in Fig. 5a. The black curve represents the φ changing by L_v with L_h of 3, while the red curve represent the φ changing by L_h with L_v of 20. The φ increased linearly by increasing L_v, and can reach 65.3° when L_v is 20. Conversely, φ decreases sharply from 79.2° with increasing L_h, then stabilizes around 5°. Therefore, in practical applications of morphing structures, a larger bending angle

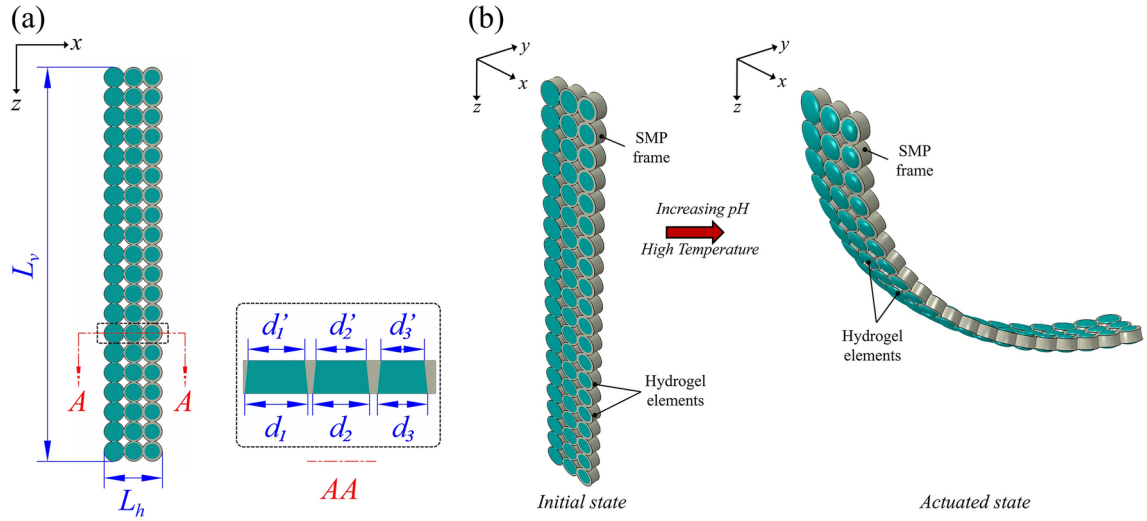

Fig. 6. The shape-morphing structure: curling building block (**a**) structural design (**b**) working principle.

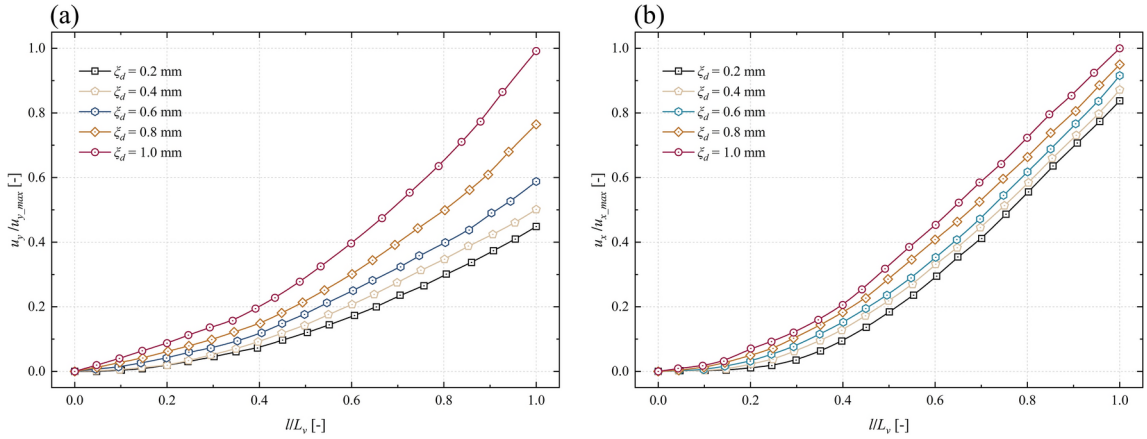

Fig. 7. The curling performance affected by different diameter difference (ξ_d). (**a**) The displacement ratio in y direction. (**b**) The displacement ratio in x direction.

can be achieved by increasing the number of vertical layers and reducing the number of horizontal layers. The bending performance affected by the thickness difference is shown in Fig. 5b. As ξ_t increased from 0.1 mm to 0.5 mm, φ rose sharply from 53.2° to 85.4°. Besides, as ξ_t further increased from 0.5 mm to 1 mm, φ gradually increased from 85.6° to 92.5°. Thus, increasing the thickness difference between SMP covers also improves the morphing structure's bending performance.

In addition to bending, the structure need to achieve complicated deformation with increased degrees of freedom to satisfied the industrial requirements. The intelligent structure can also facilitate the assembly of the building block of curling configuration, was shown in Fig. 6. The structural design is depicted in Fig. 6a. The building block of the curling configuration resembles a bending configuration but differs by using a cone frustum hydrogel unit with varying diameters at its top (d_i') and bottom (d_i) surfaces. Moreover, only the diameter on the top side will be changed in the curling configuration, while the diameter on the bottom side will remain consistent with the diameter used in the bending configuration. The thickness difference between two surface (ξ_d) can be expressed as,

$$d_i\prime - d_i = \xi_d \tag{17}$$

The working principle is shown in Fig. 6b. Initially, the morphing structure remains straight. Upon actuation of the hydrogel unit, volumetric changes induce bending in the x direction. Additionally, due to the cone frustum shape, differential swelling on the front and back sides causes bending in the y direction. Consequently, the morphing structure achieves a curling deformation by combining these bending behaviours in multiple directions, and the curling deformation is characterized by the displacements in the free end.

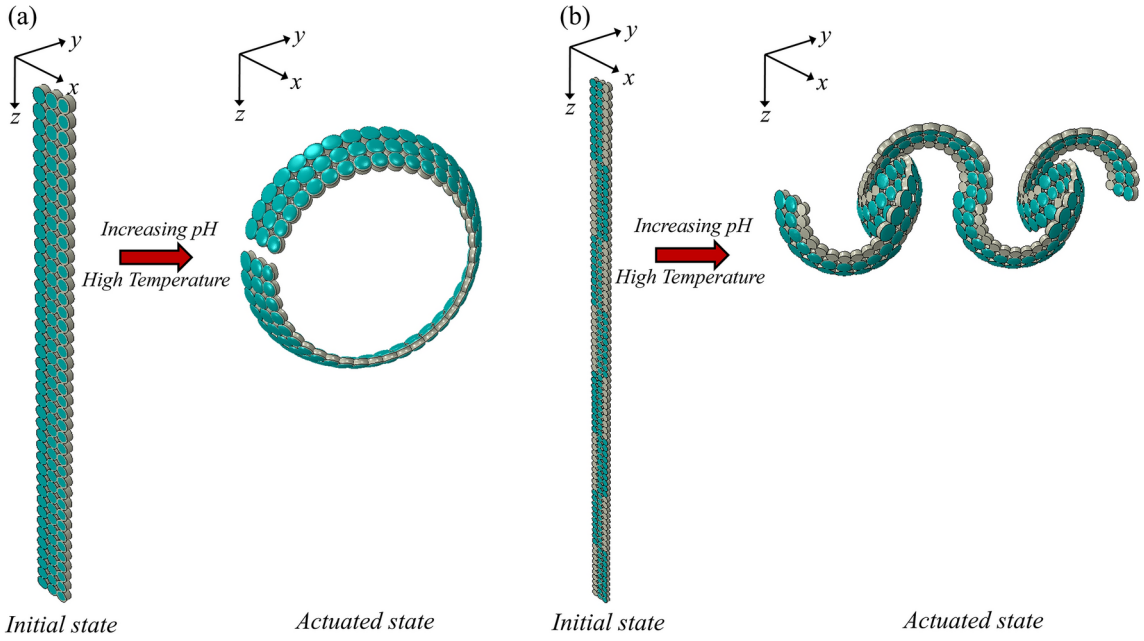

Fig. 8. Different applications of curling configuration. (**a**) Large deformation for pipeline installation and maintenance. (**b**) Exploration of the space.

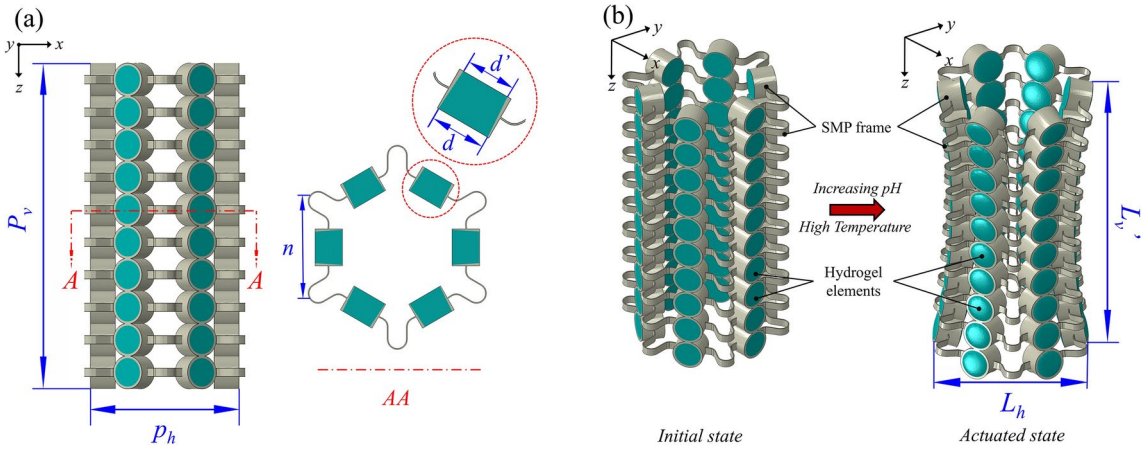

Fig. 9. The shape-morphing structure: elongation mode (**a**) structural design (**b**) working principle.

The curling performance affected by different ξ_d is explored shown in Fig. 7. Figure 7a shows the displacement ratio in the y direction along the structure. As ξ_d increases, the displacement in the y direction not only increases but does so at an accelerating rate. This indicates that increasing ξ_d significantly enhances bending deformation in the y direction. Figure 7b describes the displacement ratio in the x direction along the structure. As ξ_d increases, the displacement in the x direction gradually increases but remains minimal, indicating that ξ_d has a limited effect on bending deformation in the x direction. Combined with the bending behaviors shown in Fig. 4, in the curling configuration, bending deformations in different directions appear relatively independent. Therefore, ξ_d and ξ_t are the independent input to design the different morphing structure of curling configuration with varying bending deformations in different directions.

More complex deformations can be achieved through the curling configuration, as demonstrated in Fig. 8. Figure 8a illustrates that by increasing the number of layers in the structure, a ring shape is formed. This ring-shaped structure is suitable for applications such as underwater pipeline installation and maintenance. Additionally, Fig. 8b shows that by reversing the arrangement of the layers, an S-shaped structure is produced. This S-shaped structure is useful for seabed exploration.

Furthermore, the intelligent structure can form three-dimensional (3D) building block that achieve elongation deformations to satisfy the requirement of space exploration underwater, which shown in Fig. 9. The structural design is shown in Fig. 9a. The intelligent units placed symmetrical in one layer and linked by SMP frame, and using multiple layers of units to form the 3D structure. The lengths of the structure in x direction and

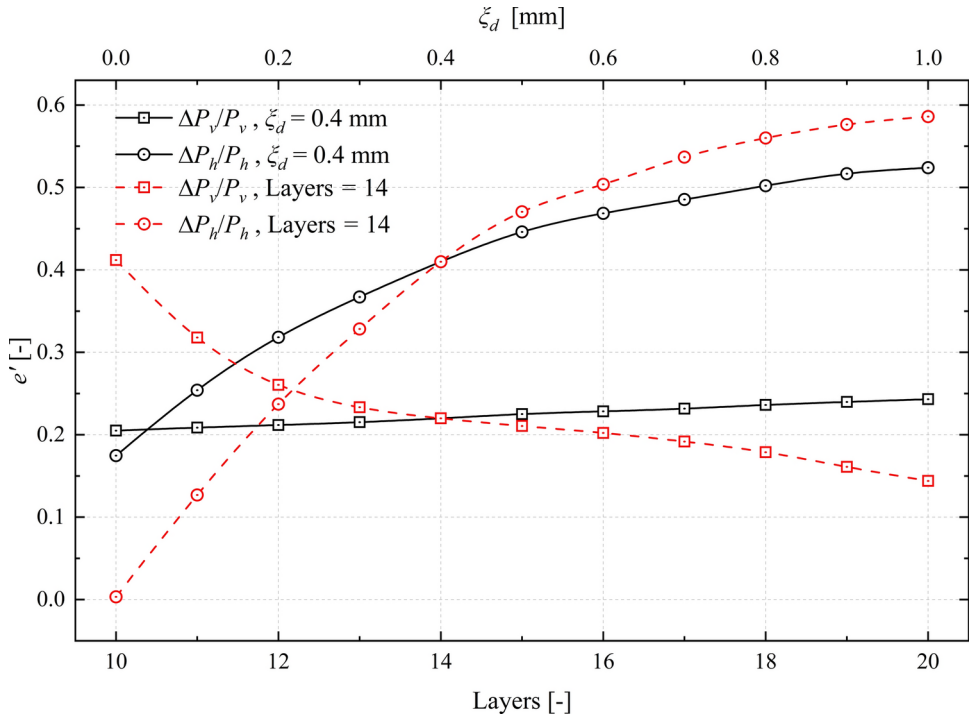

Fig. 10. The elongation performance affected by actuator layers and actuator diameter difference (ξ_d).

z direction are P_h and P_v, respectively. Besides, the distance between the SMP links is n of 28 mm, the diameters of cone frustum hydrogel unit at top and bottom side are d_e and d_e', respectively, and set d_e' with a fixed value of 9.8 mm. The diameter difference is also expressed as ξ_d. The elongation configuration's working principle is illustrated in Fig. 9b. Initially, the structure is cylindrical. Upon activating the units, the structure elongates due to the swelling of the hydrogel units. Concurrently, the difference in diameter causes each branch to bend. Consequently, the actuated state results in an elongated dumbbell-like structure. The elongation performance is described by the changes in the length, which can be expressed as,

$$\Delta P_h = P_h' - P_h \tag{18}$$

$$\Delta P_v = P_V' - P_V \tag{19}$$

where P_h' and P_v' are the elongated length in x direction and z direction, respectively. In addition, the length change is normalized as a dimensionless number e', which is expressed as $\Delta P/P$.

The elongation performance affected by actuator layers and ξ_d is shown in Fig. 10. As the amount of layers increases, e' increases significantly in the x direction but less in the z direction, which indicates that the elongation in the vertical direction is largely independent of the structure's length, whereas the elongation in the horizontal direction is highly sensitive to variations in the structure's length. In addition, as ξ_d increases, e' decreases sharply from 0.0 mm to 0.3 mm and then gradually from 0.3 mm to 1.0 mm in the z direction. Conversely, e' increases sharply in the x direction. Thus, diameter differences negatively impact elongation in the vertical direction and affect elongation sensitivity in the horizontal direction.

Stiffness variation of the morphing structure

The SMP applied in the morphing structures is used for stabilizing the hydrogels and achieving the stiffness variation. The bending stiffness (S_a) of the structure of bending configuration is analyzed to evaluate the stiffness of the structure, which can be expressed as,

$$S_a = \frac{F_E L_S \sin\beta^\circ}{\theta^\circ} \tag{20}$$

as shown in Fig. 11a, F_E illustrates the external force, L_s is the distance from the top end to the bending point. Thus, F_E L_S sinβ is the external moment about the top end. In addition, θ illustrates the rotational angle caused by the external moment.

To evaluate the effects of the stiffness variation of SMP, a comprehensive comparison of proposed morphing structure and other actuators is analyzed in Fig. 11b, which includes particle-based actuator[6], particle jamming

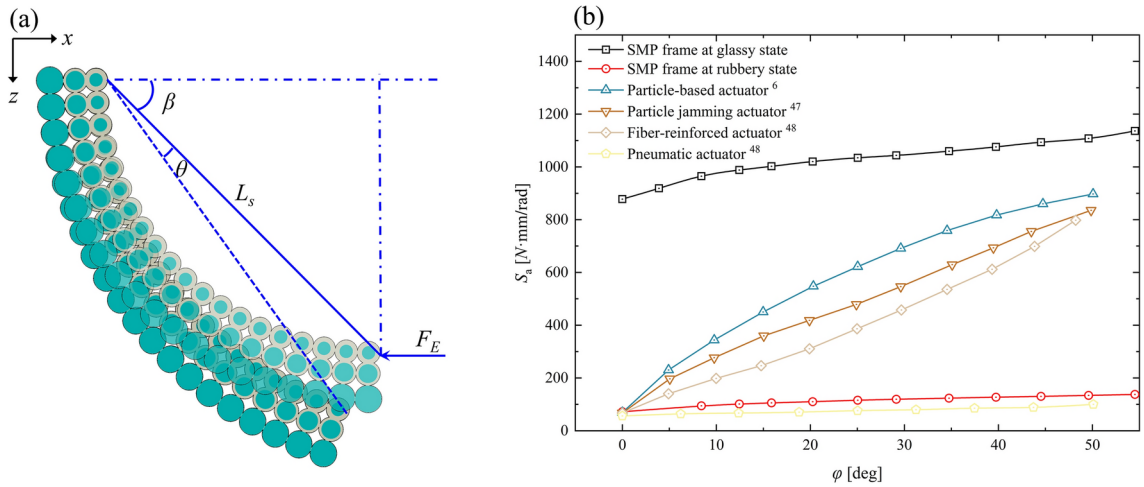

Fig. 11. The bending stiffness illustration and analysis (**a**) Illustration of the calculation of the bending stiffness. (**b**) The bending stiffness (S_a) comparison of different actuators.

actuator[47], fiber-reinforced actuator[48], and pneumatic actuator[48]. Additionally, temperatures of 360 K and 295 K are established for the SMP in its rubbery and glassy states, respectively. The proposed morphing structure exhibits a stiffness in the glassy state that is 10 times greater than in the rubbery state, demonstrating the effectiveness of the phase transition in SMP for varying stiffness. Additionally, this structure surpasses others, maximum with a stiffness up to 1.2 times higher than the particle-based actuator, 1.35 times higher than the particle jamming actuator, 1.42 times higher than the fiber-reinforced actuator, and 11.3 times higher than the pneumatic actuator. These findings indicate that employing an SMP frame is a highly effective method for enhancing structural stiffness.

Conclusion

Developing morphing structures based on soft actuators is crucial for enabling soft robots to perform complex deformations and actions. In this study, we employed smart materials, including pH-sensitive hydrogel and shape memory polymer (SMP), to create the intelligent structures as the building block. Based on the building blocks, the model-based design approach was used to develop intelligent morphing structures applicable to maritime engineering.

The proposed mechanically intelligent structure achieves active deformation which is characterized by numerical model. The simulation results relating to the hyperplastic behaviors of shape memory polymers (SMP) and pH-sensitive hydrogels are matchable with experimental data, which proves the feasibility of the materials model. The cylindrical intelligent structure combining SMP with pH-sensitive hydrogels is able to change in the volume and the be stiffness. Actuation occurs through an increase in pH, while stiffness enhancement is achieved by lowering the temperature.

The development of tailored morphing structures capable of bending, curling, and elongation is achieved through the use of variable intelligent structures with diverse designs. The bending and curling configurations utilize multi-layer hydrogel units within a SMP frame, while the elongation configuration comprises hydrogel units, an SMP frame, and connecting elements. Bending performance is assessed by the bending angle, which increases with the number of vertical layers and thickness differences, but decreases with the number of horizontal layers. Curling performance is measured by displacements in various directions, predominantly influenced by axial thickness differences and minimally by vertical thickness differences. Elongation performance is evaluated by the elongation ratio, which increases horizontally with both thickness differences and the number of layers, but decreases vertically with thickness differences.

Using SMP as the morphing structure frame effectively enables stiffness variation. In its rubbery state, the bending stiffness of the proposed structure is slightly higher than that of a pneumatic actuator. However, once the SMP transitions to its glassy state, the bending stiffness increases tenfold compared to the rubbery state, exceeding particle-based, particle jamming, and fiber-reinforced actuators.

The higher pH of seawater compared to air is ideal for actuating pH-sensitive hydrogels, and the waste heat generated during subsea operations can effectively drive SMPs. This makes the proposed structure highly suitable for underwater applications and subsea operations, supporting various morphing structures. Future research will focus on developing an enhanced methodology grounded in model-based design principles. This methodology will integrate theoretical frameworks with experimental validation, streamlining the development of products through systematic design and manufacturing procedures for maritime and underwater applications. Besides, the controlling system will be involved into the feedback process to achieve the real-time control, which will improve the adaptability of the designs.

Data availability

The datasets generated during and/or analysed during the current study are available from the corresponding author on reasonable request.

Received: 29 June 2024; Accepted: 24 September 2024
Published online: 30 October 2024

References

1. Yarali, E. et al. Magneto-/electro-responsive polymers toward manufacturing, characterization, and biomedical/soft robotic applications. *Appl. Mater. Today* **26**, 101306 (2022).
2. Hartmann, F., Baumgartner, M. & Kaltenbrunner, M. Becoming sustainable, the new frontier in soft robotics. *Adv. Mater.* **33**, 2004413 (2021).
3. Aracri, S. et al. Soft robots for ocean exploration and offshore operations: A perspective. *Soft Rob.* **8**, 625–639 (2021).
4. Haghiashtiani, G., Habtour, E., Park, S.-H., Gardea, F. & McAlpine, M. C. 3D printed electrically-driven soft actuators. *Extrem. Mech. Lett.* **21**, 1–8 (2018).
5. Huang, W., Xiao, J. & Xu, Z. A variable structure pneumatic soft robot. *Sci. Rep.* **10**, 18778 (2020).
6. Chen, Q., Schott, D. & Jovanova, J. Conceptual design of a novel particle-based soft grasping gripper. *J. Mech. Robot.* **10**(1115/1), 4062647 (2024).
7. Villeda-Hernandez, M. et al. Chemically driven oscillating soft pneumatic actuation. *Soft Rob.* **10**, 1159–1170 (2023).
8. Tariq, A. et al. Recent advances in the additive manufacturing of stimuli-responsive soft polymers. *Adv. Eng. Mater.* **25**, 2301074 (2023).
9. Bahl, S., Nagar, H., Singh, I. & Sehgal, S. Smart materials types, properties and applications: A review. *Mater. Today Proc.* **28**, 1302–1306 (2020).
10. Terryn, S. et al. A review on self-healing polymers for soft robotics. *Mater. Today* **47**, 187–205 (2021).
11. Khalid, M. Y. et al. 3D printing of magneto-active smart materials for advanced actuators and soft robotics applications. *Eur. Polymer J.* **205**, 112718 (2024).
12. Sachyani Keneth, E., Kamyshny, A., Totaro, M., Beccai, L. & Magdassi, S. 3D printing materials for soft robotics. *Adv. Mater.* **33**, 2003387 (2021).
13. Lutolf, M. P. Spotlight on hydrogels. *Nat. Mater.* **8**, 451–453 (2009).
14. Mao, Y. et al. 3D printed reversible shape changing components with stimuli responsive materials. *Sci. Rep.* **6**, 24761 (2016).
15. Zheng, J. et al. Mimosa inspired bilayer hydrogel actuator functioning in multi-environments. *J. Mater. Chem. C* **6**, 1320–1327 (2018).
16. Duan, J., Liang, X., Zhu, K., Guo, J. & Zhang, L. Bilayer hydrogel actuators with tight interfacial adhesion fully constructed from natural polysaccharides. *Soft Matter* **13**, 345–354 (2017).
17. Takashima, Y. et al. Expansion–contraction of photoresponsive artificial muscle regulated by host–guest interactions. *Nat. Commun.* **3**, 1270 (2012).
18. Palleau, E., Morales, D., Dickey, M. D. & Velev, O. D. Reversible patterning and actuation of hydrogels by electrically assisted ionoprinting. *Nat. Commun.* **4**, 2257 (2013).
19. Shen, Q. et al. A multiple-shape memory polymer-metal composite actuator capable of programmable control, creating complex 3D motion of bending, twisting, and oscillation. *Sci. Rep.* **6**, 24462 (2016).
20. Aksoy, B. & Shea, H. Multistable shape programming of variable-stiffness electromagnetic devices. *Sci. Adv.* **8**, eabk0543 (2022).
21. Khalid, M. Y. et al. Shape-memory and self-healing properties of sustainable cellulosic nanofibers-based hybrid materials for novel applications. *Giant* https://doi.org/10.1016/j.giant.2024.100299 (2024).
22. Xia, Y., He, Y., Zhang, F., Liu, Y. & Leng, J. A review of shape memory polymers and composites: Mechanisms, materials, and applications. *Adv. Mater.* **33**, 2000713 (2021).
23. Gandhi, F. & Kang, S.-G. Beams with controllable flexural stiffness. *Smart Mater. Struct.* **16**, 1179 (2007).
24. Wang, W., Yu, C. Y., Abrego Serrano, P. A. & Ahn, S.-H. Shape memory alloy-based soft finger with changeable bending length using targeted variable stiffness. *Soft Robot.* **7**, 283–291 (2020).
25. Zhang, Y. et al. Progress, challenges, and prospects of soft robotics for space applications. *Adv. Intell. Syst.* **5**, 2200071 (2023).
26. Iida, F. & Laschi, C. Soft robotics: Challenges and perspectives. *Proced. Comput. Sci.* **7**, 99–102 (2011).
27. Hawkes, E. W., Majidi, C. & Tolley, M. T. Hard questions for soft robotics. *Sci. Robot.* **6**, eabg6049 (2021).
28. Lipson, H. Challenges and opportunities for design, simulation, and fabrication of soft robots. *Soft Robot.* **1**, 21–27 (2014).
29. Mengaldo, G. et al. A concise guide to modelling the physics of embodied intelligence in soft robotics. *Nat. Rev. Phys.* **4**, 595–610 (2022).
30. Polygerinos, P. et al. Modeling of soft fiber-reinforced bending actuators. *IEEE Trans. Robot.* **31**, 778–789 (2015).
31. Nguyen, P. H. & Zhang, W. Design and computational modeling of fabric soft pneumatic actuators for wearable assistive devices. *Sci. Rep.* **10**, 9638 (2020).
32. Song, J. et al. Octopus-inspired adaptable soft grippers based on 4D printing: Numerical modeling, inverse design, and experimental validation. *Adv. Intell. Syst.* **5**, 2200384 (2023).
33. Li, Q. *Modeling and Finite Element Analysis of Smart Materials* (North Carolina State University, 2006).
34. Ganji, F., Vasheghani, F. S. & Vasheghani, F. E. Theoretical description of hydrogel swelling: a review. *Iran. Polym. J.* **19** (5), 375–398 (2010).
35. Flory, S. M., Phillips Jr, T. J., Reidenbach, R. E. & Robin, D. P. A multidimensional analysis of selected ethical issues in accounting. *Account. Rev.* **1992**, 284–302 (1992).
36. Huggins, C., Stevens, R. & Hodges, C. V. Studies on prostatic cancer: II. The effects of castration on advanced carcinoma of the prostate gland. *Arch. Surg.* **43**, 209–223 (1941).
37. Marcombe, R. et al. A theory of constrained swelling of a pH-sensitive hydrogel. *Soft Matter* **6**, 784–793 (2010).
38. Haseebuddin, S., Raju, K. & Yaseen, M. Applicability of the WLF equation to polyurethane polyols and film properties of their resins. *Progress Org. Coat.* **30**, 25–30 (1997).
39. Rudolph, N. M., Agudelo, A. C., Granada, J. C., Park, H. E. & Osswald, T. A. WLF model for the pressure dependence of zero shear viscosity of polycarbonate. *Rheol. Acta* **55**, 673–681 (2016).
40. Ward, I. M. & Sweeney, J. *Mechanical Properties of Solid Polymers* (Wiley, 2012).
41. Khalid, M. Y. et al. 3D/4D printing of cellulose nanocrystals-based biomaterials: Additives for sustainable applications. *Int. J. Biol. Macromol.* **251**, 126287 (2023).
42. Wang, J., Kean, R., Randall, J. & Giles, D. The effect of crystallinity on the rheological behavior of poly (lactide). *Int. J. Polym. Anal. Charact.* **4**, 393–405 (1998).
43. Al-Rubaiai, M., Pinto, T., Qian, C. & Tan, X. Soft actuators with stiffness and shape modulation using 3D-printed conductive polylactic acid material. *Soft Robot.* **6**, 318–332 (2019).
44. Eichenbaum, G. M., Kiser, P. F., Dobrynin, A. V., Simon, S. A. & Needham, D. Investigation of the swelling response and loading of ionic microgels with drugs and proteins: The dependence on cross-link density. *Macromolecules* **32**, 4867–4878 (1999).

45. Liu, Y., Gall, K., Dunn, M. L., Greenberg, A. R. & Diani, J. Thermomechanics of shape memory polymers: Uniaxial experiments and constitutive modeling. *Int. J. Plasticity* **22**, 279–313 (2006).
46. Qi, H. J., Nguyen, T. D., Castro, F., Yakacki, C. M. & Shandas, R. Finite deformation thermo-mechanical behavior of thermally induced shape memory polymers. *J. Mech. Phys. Solids* **56**, 1730–1751 (2008).
47. Li, Y., Chen, Y., Yang, Y. & Li, Y. Soft robotic grippers based on particle transmission. *IEEE/ASME Trans. Mechatron.* **24**, 969–978 (2019).
48. Jiang, P., Yang, Y., Chen, M. Z. & Chen, Y. A variable stiffness gripper based on differential drive particle jamming. *Bioinspiration Biomim.* **14**, 036009 (2019).

Acknowledgements

This work is supported by the National Natural Science Foundation of China Grant No. 52071240 and China Scholarship Council Grant No. 202006950011. The financial contributions are gratefully acknowledged.

Author contributions

Q.C. and J.J. designed the model and the framework, analysed the data, and carried out the implementation. Q.C. performed the calculations and wrote the manuscript. J.J and D.S. conceived the study and were in charge of overall direction and planning. All authors reviewed the manuscript.

Competing interests

The authors declare no competing interests.

Additional information

Correspondence and requests for materials should be addressed to Q.C.

Reprints and permissions information is available at www.nature.com/reprints.

Publisher's note Springer Nature remains neutral with regard to jurisdictional claims in published maps and institutional affiliations.